

# K $-^3\text{He}$ self-compensating co-magnetometer for tests of CPT symmetry

Michael Romalis, Joel Allred, and Robert Lyman

*Department of Physics, University of Washington, Seattle, WA 98195*

We describe a new K- $^3\text{He}$  co-magnetometer designed for tests of CPT and local Lorentz symmetries. The K magnetometer operates at a high number density with a long transverse spin relaxation time by eliminating spin relaxation due to K-K spin-exchange collisions. The polarization of  $^3\text{He}$  is detected by its interaction with K atoms. The co-magnetometer is operated in a self-compensating mode so that magnetic field drifts do not contribute to the signal. It is sensitive only to a spin coupling that does not scale with the magnetic moment. The principle of operation and performance of the device are discussed.

## 1 Introduction

CPT symmetry has traditionally been tested by comparing the properties of particles and anti-particles, such as their masses, magnetic moments, decay rates, etc. While such tests are intuitively obvious, recent theoretical work by Alan Kostelecky and co-workers showed that CPT violation can be detected without the use of anti-particles. While CPT-violating effects necessarily require a breakdown of the standard field theory formalism at some energy, they can be represented in the low energy effective field theory by a vector field with a non-zero expectation value. This field defines a preferred direction in space, and thus also breaks the Lorentz symmetry. The CPT-violating field interacts with spins of ordinary particles in a way similar to the magnetic field. Because of its vector character, the interaction can be modulated by changing the orientation of the spin and does not require comparison with anti-particles. Assuming that the coupling to the spin does not scale with the magnetic moment, it can be distinguished from the magnetic field by comparing the energy shifts for two different types of particles. The sensitivity to CPT-violating effects is simply determined by the absolute energy resolution of the measurement<sup>1</sup>. Therefore such tests are ideally suited for atomic magnetometers, which already hold a record for the lowest measured energy shift of  $10^{-33}\text{GeV}$ <sup>2</sup>.

This physics motivation lead us to design a dedicated experiment optimized to search for CPT violation. It is based on an alkali-metal – noble gas co-magnetometer, the first to be used for a precision measurement. The use of an alkali metal offers several advantages. Its spin precession signal can be measured by detecting photons with high quantum efficiency. For our condi-

tions the transverse spin relaxation rate of the alkali-metal spins is limited by the spin-destruction processes, not much faster spin-exchange rate, giving long spin relaxation times at high alkali-metal densities. Spin exchange between the alkali-metal and noble gas atoms is used to polarize the noble gas spins and detect their precession signal. The cross-section for collisions between alkali-metal and noble-gas atoms has a real component  $\sigma_1$  responsible for the transfer of angular momentum and an imaginary component  $\sigma_2$  that produces a frequency shift. The ratio  $\sigma_2/\sigma_1$  is on the order of  $10^5$ , which implies that in principle the frequency shift from a single noble gas atom can be measured with a signal to noise ratio much greater than unity.

Using the frequency shift produced by polarized noble gas atoms on the alkali-metal atoms, the magnetometer can be operated in a "self-compensating" mode in which the magnetic field fluctuations are automatically canceled. Only a non-magnetic interaction that does not scale with the magnetic moments of the atoms can produce a first order signal.

## 2 Alkali-metal magnetometer

### 2.1 Theory of operation

The fundamental energy sensitivity of an atomic magnetometer in a given measurement time  $t$  is determined by the spin coherence time  $T_2$  and the total number of atoms  $N$ ,

$$\delta E = \frac{\hbar}{\sqrt{T_2 N t}}. \quad (1)$$

For alkali-metal magnetometers the transverse spin relaxation time is determined by several processes. In general, it can be written as

$$\frac{1}{T_2} = n_a \langle \bar{v}_{aa} \sigma_{se}^a \rangle + n_a \langle \bar{v}_{aa} \sigma_{sd}^a \rangle + \sum_b n_b \langle \bar{v}_{ab} \sigma_{sd}^b \rangle + D_{ab} S \left( \frac{\pi}{R} \right)^2, \quad (2)$$

where  $\sigma_{se}^a$ ,  $\sigma_{sd}^a$ , and  $\sigma_{sd}^b$  are the alkali-metal spin-exchange, alkali-metal spin destruction, and buffer gas spin destruction cross-sections,  $\bar{v}$ 's are the relative velocities, and  $n$ 's are the number densities of the atoms. The sum runs over all buffer gases present in the cell (for example,  $^3\text{He}$  and  $\text{N}_2$ ).  $D_{ab}$  is the mutual diffusion constant,  $R$  the radius of the spherical cell.  $S$  is the nuclear spin slowing-down factor which takes into account the fact that spin relaxation near the walls destroys not only electron, but also nuclear spin polarization<sup>3</sup>.

For high alkali-metal number density the spin-exchange contribution to the transverse relaxation rate usually dominates, because the cross-section  $\sigma_{se}^a \simeq 2 \times 10^{-14} \text{cm}^2$  is much larger than the spin destruction cross-sections.

Table 1: Alkali-metal spin destruction cross-sections.

	Alkali metal ( $\sigma_{aa}$ )	$^3\text{He}$ ( $\sigma_{ab}$ )	Ne ( $\sigma_{ab}$ )	$\text{N}_2$ ( $\sigma_{ab}$ )
K	$1 \times 10^{-18} \text{cm}^2$	$8 \times 10^{-25} \text{cm}^2$	$1 \times 10^{-23} \text{cm}^2$	
Rb	$9 \times 10^{-18} \text{cm}^2$	$9 \times 10^{-24} \text{cm}^2$		$1 \times 10^{-22} \text{cm}^2$
Cs	$2 \times 10^{-16} \text{cm}^2$	$3 \times 10^{-23} \text{cm}^2$		$6 \times 10^{-22} \text{cm}^2$

However, spin-exchange is not inherently a limiting factor for transverse spin relaxation, since the total angular momentum of the colliding atoms is conserved. The gyromagnetic ratio for atoms in the  $F = I \pm 1/2$  states is approximately equal to  $\gamma = \pm g_B \mu_B / (2I + 1) \hbar$  and spin polarizations in the two hyperfine states precess in opposite directions. The relaxation is caused by the transfer of atoms between hyperfine states which have different expectation values of  $m$ . However, as was first observed in <sup>4</sup>, at high densities and low magnetic field, such that  $n_a \langle v_{aa} \sigma_{se}^a \rangle \gg \gamma B$ , the spin exchange contribution to the transverse relaxation rate is eliminated. Very fast spin exchange between the two hyperfine states forces atoms to precess in the same direction and causes  $\langle m \rangle$  to be the same in the two states <sup>5</sup>. In this limit the gyromagnetic ratio is the same for the two hyperfine states, but it is reduced from the low spin-exchange limit,

$$\gamma = \frac{3g_B \mu_B}{(3 + 4I(I + 1)) \hbar}. \quad (3)$$

The remaining spin relaxation rate is due to the spin-destruction collisions and diffusion to the walls. Table 1 summarizes measured spin-destruction cross-sections for several alkali metals and buffer gases. The spin destruction cross-sections for the K-<sup>3</sup>He pair are an order of magnitude or more smaller than for other possible combinations. The optimal buffer gas density of about 3 atm. is determined by the trade-off between spin destruction and diffusion contributions.

## 2.2 Experimental Implementation

Our experimental arrangement is shown in Figure 1. K atoms are contained in a 1" dia. thin-walled spherical cell made from GE180 aluminosilicate glass. For tests of the K magnetometer the cell contains a mixture of 3 atm. of <sup>4</sup>He and 30 torr of N<sub>2</sub>. The cell is located in an oven constructed from high-temperature G-7 fiberglass and heated to 190 °C by flowing hot air. It is surrounded by 5-layer cylindrical magnetic shields with a shielding factor of 10<sup>6</sup>. A set of coils inside the shields allows us to control of the magnetic fields and first order gradients. K atoms are optically pumped by a 1W multi-mode

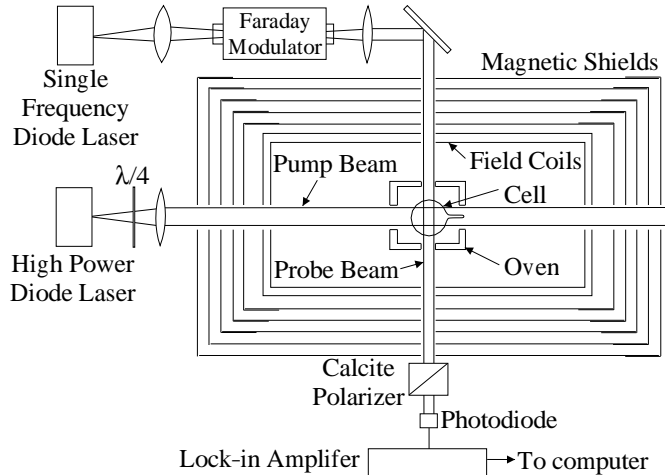


Figure 1: A schematic of the K magnetometer setup.

diode laser. A single frequency diode laser directed perpendicular to the pump beam is used for detection of the spin polarization. The component of the K spin polarization parallel to the direction of the probe beam is measured using optical rotation. We use a polarization modulation technique to move the signal away from  $1/f$  noise of the detectors. The plane of polarization of the probe laser is modulated by a Faraday rotator with an amplitude  $\alpha = 2^\circ$  at a frequency of  $\omega_m = 2\pi \times 3$  kHz. The light then passes through a calcite linear polarizer set for maximum extinction. The transmitted signal is given by

$$I = I_0 \sin[\alpha \sin(\omega_m t) + \phi]^2 \simeq I_0[\alpha^2 \sin^2(\omega_m t) + 2\phi\alpha \sin(\omega_m t)], \quad (4)$$

where  $\phi$  is the optical rotation angle proportional to the component of K spin polarization along the probe beam. The signal at the first harmonic of the modulation frequency is detected with a lock-in amplifier.

To measure the spin relaxation time we use a synchronous pumping technique. A small vertical magnetic field is applied perpendicular to both pumping and probing beams and the pumping beam is chopped at a frequency close to the resonance condition given by Eq. (3). The precession of the polarization around the vertical field is detected using the probe beam. One such resonance is shown in Figure 2 for  $n_K = 10^{14} \text{ cm}^{-3}$  and  $n_{He} = 8 \times 10^{19} \text{ cm}^{-3}$ . The width of the resonance gives the transverse spin relaxation time. The resulting value  $T_2 = 45$  msec is in excellent agreement with the value calculated from Eq.

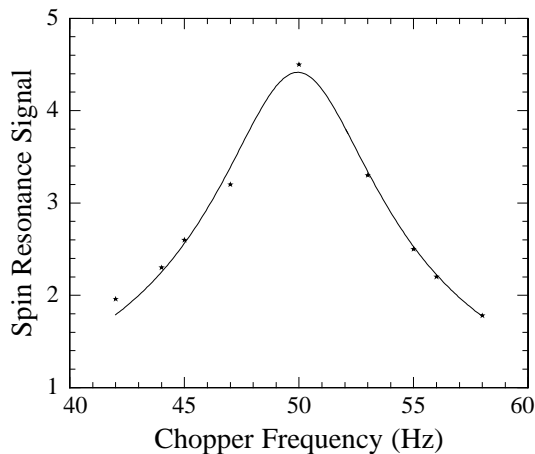


Figure 2: Synchronous pumping resonance. The fit based on the lineshape calculated in <sup>6</sup> gives  $T_2 = 45$  msec.

(2) using known spin-destruction rates, but omitting the spin-exchange term which would give a  $T_2 = 7 \mu\text{sec}$ . This demonstrates the elimination of the spin-exchange relaxation at low magnetic fields.

The theoretical sensitivity of the magnetometer can be estimated from Eq. (1). Assuming shot noise -limited detection, it gives a magnetic field sensitivity of  $0.01 \text{ fT}/\sqrt{\text{Hz}}$ , about 2 orders of magnitude better than the sensitivity of the best existing atomic and SQUID magnetometers, which are largely limited by fundamental noise sources.

For direct tests of the magnetic field sensitivity we adjust all three components of the magnetic field to zero. In a zero field the K spins are polarized along the direction of the pumping beam, but are easily rotated in the plane of the laser beams by a small vertical magnetic field<sup>7</sup>. This rotation is measured by the probe beam. To determine the sensitivity of the magnetometer, we apply a small known modulation to the vertical magnetic field at a frequency of 10-20 Hz and record the frequency spectrum of the rotation signal measured by the lock-in amplifier. In this way we determine the magnetic field calibration of the signal and its spectral noise density. Our preliminary measurements give a magnetic field noise level of  $10 \text{ fT}/\sqrt{\text{Hz}}$  that is rather insensitive to various operating parameters. This noise level is most likely dominated by the thermal Johnson currents flowing in the magnetic shields<sup>8</sup>. To achieve this level of noise we had to remove nearly all conducting materials from the inside of the

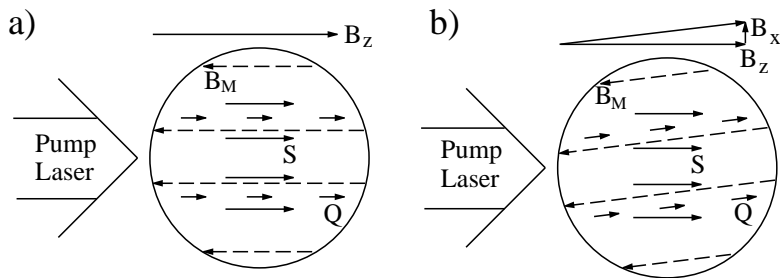


Figure 3: Self-compensating operation: a) perfect alignment of the magnetic field, b) response to a small vertical magnetic field  $B_x$ . Here  $S$  denotes K electron spin,  $Q$  denotes  $^3\text{He}$  nuclear spin, and  $B_M$  is the effective magnetic field felt by K atoms due to  $^3\text{He}$  polarization.

shields. The magnetic field noise produced by thermal currents in magnetic shields has been calculated and measured in<sup>8</sup> for a flat slab geometry. The calculation for a cylindrical shield is more complicated, but our estimates give a noise level consistent with  $10 \text{ fT}/\sqrt{\text{Hz}}$ . We are presently testing a gradiometer setup, where the probe beam is detected by several detectors and the magnetic field is measured independently in different parts of the cell. The noise in the magnetic field gradient should be substantially smaller, and we have already observed a factor of 2 reduction in the noise of the gradiometer.

### 3 $^3\text{He}$ co-magnetometer

#### 3.1 Theory of operation

$^3\text{He}$  gas has a great potential as a magnetic sensor, since one can easily obtain spin relaxation times of several hundreds of hours and very high number densities of  $2 \times 10^{20} \text{ cm}^{-3}$ .  $^3\text{He}$  is polarized by spin-exchange with optically pumped K atoms that are also used as an efficient detector of the  $^3\text{He}$  magnetization. For  $^3\text{He}$  contained in a spherical cell with a uniform polarization the effective magnetic field seen by K atoms is

$$B_M = \frac{8\pi}{3} \kappa_0 M, \quad (5)$$

where  $M$  is the classical magnetization of polarized  $^3\text{He}$  and  $\kappa_0 \simeq 6$  is an enhancement factor due to attraction of the K electron wavefunction to the  $^3\text{He}$  nucleus<sup>9</sup>. This field is typically on the order of a few mG.

One of the main advantages of the K- $^3\text{He}$  co-magnetometer for a CPT search is the possibility of operation in a self-compensating mode making it

insensitive to magnetic field fluctuations. The operation is illustrated in Figure 3. An axial magnetic field  $B_z$  is applied along the pump beam direction equal in magnitude and opposite in sign to  $B_M$  (the relative sign of  $B_M$  and  $B_z$  is set by the sense of the circular polarization of the K pumping light). Thus, the K magnetometer operates in a zero magnetic field, as described above. But  $^3\text{He}$  atoms do not see their own classical magnetization field (given by Eq. (5) with  $\kappa_0 = 1$ ) because it comes entirely from the  $\delta$  function part of the classical dipolar magnetic field and two  $^3\text{He}$  atoms cannot occupy the same point in space. Thus,  $^3\text{He}$  atoms only see the applied field  $B_z$ , which is sufficient to prevent spin relaxation of  $^3\text{He}$  due to magnetic field gradients. Now consider the response of the magnetometer to a small slowly varying vertical field  $B_x$ . Here we also include the CPT violating fields  $b_x^e$  and  $b_x^{He}$  coupling only to the electron and the  $^3\text{He}$  spins, respectively. For slow variations of  $B_x$ , the  $^3\text{He}$  polarization will follow adiabatically the total field and will tilt from the  $z$  axis by an angle

$$\beta = (B_x + b_x^{He}/\mu_{He})/B_z \ll 1. \quad (6)$$

The vertical magnetic field seen by the K magnetometer will be

$$B_{Kx} = B_x + B_M(B_x + b_x^{He}/\mu_{He})/B_z + b_x^e/(g_s\mu_0) = -b_x^{He}/\mu_{He} + b_x^e/(g_s\mu_0), \quad (7)$$

where we used the fact that  $B_M = -B_z$ . Thus, the magnetometer automatically compensates for changes in the magnetic field and is only sensitive to CPT violating effects to the extent that they do not scale with the magnetic moments of the particles.

### 3.2 Experimental Implementation

The setup for co-magnetometer operation is exactly the same as discussed above, only with  $^3\text{He}$  buffer gas in the cell. The longitudinal spin relaxation time of  $^3\text{He}$  in our cells is about 300 hours, dominated by dipolar  $^3\text{He}$  relaxation<sup>10</sup>. The spin exchange time with K atoms is about 40 hours. To obtain a large  $^3\text{He}$  polarization it is necessary to reduce the magnetic field gradients to less than a few  $\mu\text{G}/\text{cm}$ , since they cause an additional longitudinal spin relaxation given by:

$$\frac{1}{T_1} = D_{He} \frac{|\nabla B|^2}{B_z^2}. \quad (8)$$

We found that most non-magnetic materials, such as brass, plastic, etc., have small ferromagnetic inclusions that can become magnetized, especially when exposed to large magnetic fields.

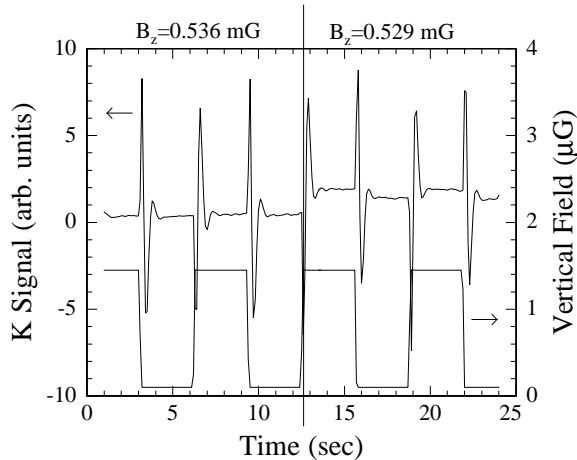


Figure 4: Response of the co-magnetometer (plotted against the left axis) to a square wave modulation of the vertical magnetic field (plotted against the right axis). The co-magnetometer is self-compensated on the left-hand side of the plot and slightly uncompensated on the right-hand side.

To start the process of the polarization, we turn up the axial magnetic field to several mG and wait for 10-20 hours to build-up the polarization. Then the field is turned down until it is equal to the magnetization field  $B_M$ , at which point the co-magnetometer is self-compensated. Figure 4 shows the response of the co-magnetometer to a square-wave modulation of the vertical field. On the left hand side the axial field was adjusted to achieve near perfect magnetic field compensation, while on the right hand side the magnetometer is slightly uncompensated. The transient spikes are due to non-adiabatic response of  $^3\text{He}$  to the rapidly changing magnetic field. Figure 5 shows the amplitude of the response to the vertical field modulation as a function of the axial magnetic field. The slope of the line can be used to determine the sensitivity of the magnetometer to CPT-violating fields using Eq. (7). Near the intercept of the line the sensitivity to slow magnetic field drifts can be suppressed by more than two orders of magnitude.

#### 4 Drifts and Systematic Errors

The co-magnetometer is designed to be operated continuously and to detect a modulation caused by the CPT-violating field as the Earth rotates around its axis. Since this is a very slow time scale, slow drifts of the experimental

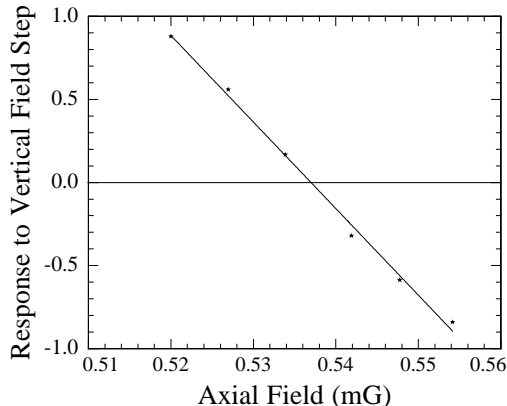


Figure 5: Amplitude of the square wave response as a function of the axial field  $B_z$ .

apparatus can cause a significant problem. While the co-magnetometer is effective in eliminating drifts of the magnetic field, several other effects can produce a false signal. One of the most significant is a relative rotation of the probe and pump beams, which gives a first-order signal. To reduce this motion we are presently designing a special non-magnetic optical table with a submerged central area for the magnetic shields. This will allow much more rigid mounting of the optics around the magnetic shields. A false signal due to relative beam motion can also be distinguished by changing the intensity of the pump light. When the optical pumping rate is much higher than the spin relaxation rate, the magnetometer becomes less sensitive to the CPT-violating fields, but remains sensitive to the beam misalignment. The motion of the beams can also be monitored by four-quadrant detectors to guard against periodic diurnal changes.

Another type of drift can be caused by slow changes in the birefringence of the cell walls, caused, for example, by temperature fluctuations. Such drift produces a rotation in the polarization plane of the probe light. This background can be subtracted by making measurements with the pump light blocked. Slow changes of the magnetic field and  $^3\text{He}$  spin polarization do not produce a first-order signal. The co-magnetometer can be kept close to the self-compensating condition by measuring its response to a vertical field. During data taking process we will periodically perform various calibration runs to control such effects.

## 5 Conclusions

We have constructed a K  $-^3\text{He}$  self-compensating co-magnetometer and demonstrated all major aspects of its operation. Based on the present measurements of the magnetic field sensitivity and assuming that the technical sources of noise discussed above can be well controlled, we expect to achieve a sensitivity of  $10^{-30}$  GeV for the electron CPT-violating coupling and  $10^{-33}$  GeV for the neutron coupling with integration times on the order of a month.

## Acknowledgements

We thank Marty Boyd and Mathew Chasan for assistance in the construction of the apparatus. This work was supported by NSF grant PHY-0098821, NIST Precision measurement grant, and University of Washington.

## References

1. V.A. Kostelecky, C. Lane, Phys.Rev. D **60**, 116010 (1999).
2. M.V. Romalis, W.C. Griffith, J.P. Jacobs, and E.N. Fortson, Phys. Rev. Lett. **86**, 2505 (2001).
3. S. Appelt, A. B. Baranga, C.J. Erickson, M.V. Romalis, A.R. Young, and W. Happer, Phys. Rev. A **58**, 1412, (1998).
4. W. Happer and H. Tang, Phys. Rev. Lett. **31** 273, (1973).
5. W. Happer and A.C. Tam, Phys. Rev. A **16**, 1877 (1977).
6. J.P. Jacobs, W.M. Klipstein, S.K. Lamoreaux, B.R. Heckel, and E.N. Fortson, Phys. Rev. A **52**, 3521 (1995).
7. S.A. Murthy, D. Krause, Jr, Z.L. Li, and L.R. Hunter, Phys. Rev. Lett. **63**, 965 (1989).
8. J. Nenonen, J. Montonen, and T. Katila, Rev. Sci. Inst. **67**, 2397 (1996).
9. M.V. Romalis and G.D. Cates, Phys. Rev A, **58**, 3004 (1998).
10. N.R. Newbury, A.S. Barton, G.D. Cates, W. Happer, and H. Middleton, Phys. Rev. A **48**, 4411 (1993).